THEORY AND ANALYSIS OF THREE-PHASE SERIES-CONNECTED PARAMETRIC MOTORS

Essam E. M. Rashad, Member IEEE
Electrical Engineering Department
Faculty of Engineering, Tanta University,
Tanta, EGYPT

Mostafa E. Abdel Karim
Electrical Engineering Department
Faculty of Engineering, Menoufia University
Shebin El-Kom, EGYPT

Yasser G. Desouky
Electrical and Control Engineering Department
Arab Academy for Science and Technology,
Miami, Alexandria, EGYPT

Abstract - **This paper presents the steady-state performance of a three phase wound-rotor parametric motor. This type of motor can be practically realized by series connection of stator and rotor phases of a conventional wound-rotor induction machine. The analysis is based on the d-q axes model, from which a phasor diagram is presented. The analysis is extended to include the magnetic saturation effect. Comparison between theoretical and experimental results showed a satisfactory agreement proving the validity of the mathematical model as well as magnetic saturation effect representation. Also the motor stability is investigated.**

Keywords: Parametric Machines, Induction motors, Wound Rotor, Synchronous Motors.

II-INTRODUCTION

The principle of operation of the parametric machine has been originally established for the generator mode when studying the behavior of periodically varying inductance *RLC* series circuits [1]. The Single phase parametric generator has been extensively studied theoretically and experimentally using different mathematical techniques based on the Floquet theory [2,3]. The three phase parametric generator has been analyzed using the d-q model [3,4], Floquet theory [3,5] and phasor diagrams [6,7].

It was found that such a machine is inherently of synchronous type allowing electromechanical energy conversion only if :

1. The rotor speed corresponds to an angular frequency of double the angular frequency of the stator mmf i.e.
$$\omega_r = 2\,\omega \qquad (1)$$
2. The series–connection of the stator and the rotor windings are such that the phase sequence of the rotor mmf is in reverse sense to that of the stator mmf as shown in Fig. 1.

Experimental and theoretical investigation for controlling the terminal voltage via the excitation capacitor has been presented [8] using a fixed thyristor controlled reactor.

96 SM 361-6 EC A paper recommended and approved by the IEEE Electric Machinery Committee of the IEEE Power Engineering Society for presentation at the 1996 IEEE/PES Summer Meeting, July 28 - August 1, 1996, in Denver, Colorado. Manuscript submitted December 29, 1995; made available for printing May 21, 1996.

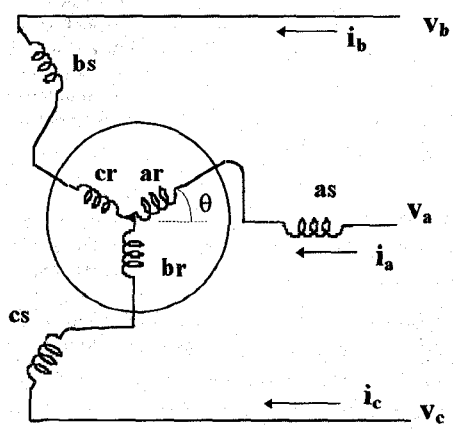

Fig. 1 ***Connection between stator and rotor windings of the parametric motor***

The parametric machine can be used as a motor or a generator depending on its terminal conditions [3]. The parametric motor has the advantage of operating at fixed speed of double the synchronous speed which depends only on the number of poles and supply frequency.

The previous work in the field of the parametric machines gave an essential attention to the generator mode of operation. Therefore, this paper is concerned with the motor mode. The aim of this paper is to :

1. propose a mathematical model for the parametric motor,
2. verify the experimental behavior to check the validity of the mathematical model and
3. investigate the limits for which the motor will be stable.

II- MATHEMATICAL MODEL

Based on the electrical connection between the balanced stator and rotor phases shown in fig. 1, the terminal voltages can be expressed as follows:

$$\left.\begin{aligned} V_a &= V_{as} + V_{ar} \\ V_b &= V_{bs} + V_{cr} \\ V_c &= V_{cs} + V_{br} \end{aligned}\right\} \qquad (2)$$

while the winding currents can be defined as follows:

$$\left.\begin{aligned} I_a &= I_{as} = I_{ar} \\ I_b &= I_{bs} = I_{cr} \\ I_c &= I_{cs} = I_{br} \end{aligned}\right\} \qquad (3)$$

The machine parameters are defined as follows:

$$\left.\begin{aligned} R_a &= R_s + R_r \\ L_a &= L_s + L_r \end{aligned}\right\} \qquad (4)$$

By writing the voltage balance equations of the six coils and substituting from equs. (2-4), the machine equations reduce to three equations describing the terminal conditions. These equations can be written in the following operational form :

$$\mathbf{V} = \mathbf{Z}(p)\,\mathbf{I} \qquad (5)$$

where $\mathbf{V} = (v_a \;\; v_b \;\; v_c)^T$ and $\mathbf{I} = (i_a \;\; i_b \;\; i_c)^T$

where T stands for the transpose operation.

$\mathbf{Z}(p)$ is the transient impedance matrix =

$$\begin{pmatrix} R_a + p\{L_a + 2M\cos(\theta)\} & p\{-0.5L_a + 2M\cos(\theta - 120°)\} & p\{-0.5L_a + 2M\cos(\theta + 120°)\} \\ p\{-0.5L_a + 2M\cos(\theta - 120°)\} & R_a + p\{L_a + 2M\cos(\theta + 120°)\} & p\{-0.5L_a + 2M\cos(\theta)\} \\ p\{-0.5L_a + 2M\cos(\theta + 120°)\} & p\{-0.5L_a + 2M\cos(\theta)\} & R_a + p\{L_a + 2M\cos(\theta - 120°)\} \end{pmatrix}$$

The periodically varying coefficients in $\mathbf{Z}(p)$ can be changed into constant coefficients by applying a synchronously rotating reference frame transformation for voltages and currents. If zero sequence quantities do not exist, the transformation factor is given by:

$$\mathbf{K}^T = \sqrt{\frac{2}{3}} \begin{pmatrix} \cos(\omega t) & \cos(\omega t - 120°) & \cos(\omega t + 120°) \\ \sin(\omega t) & \sin(\omega t - 120°) & \sin(\omega t + 120°) \end{pmatrix} \qquad (6)$$

Applying the transformation (6) to (5) yields [9]:

$$\mathbf{V}' = \mathbf{Z}'(p)\,\mathbf{I}' \qquad (7)$$

where $\mathbf{V}' = \mathbf{K}^T\mathbf{V}$, (8)

$$\mathbf{I}' = \mathbf{K}^T\mathbf{I}, \qquad (9)$$

and $\mathbf{Z}'(p) = \mathbf{K}^T\mathbf{Z}(p)\mathbf{K}$ (10)

The transformed impedance matrix $\mathbf{Z}(p)$ is given by:

$$\mathbf{Z}'(p) = \begin{pmatrix} R_a + L_d p & \omega L_q \\ -\omega L_d & R_a + L_q p \end{pmatrix} \qquad (11)$$

where

$L_d = 1.5\{L_a + 2M\}$; the direct axis inductance.

$L_q = 1.5\{L_a - 2M\}$; the quadrature axis inductance.

III- Steady-State Analysis

III-1 Voltage Balance equation

The mathematical model given by Equations (7-11) describes the dynamic behavior of the parametric motor. If the applied voltage is sinusoidal and balanced, the transformed voltages and currents are all constants. Therefore the operator p can be replaced by zero. The transformed voltage equation becomes:

$$\begin{pmatrix} V_d \\ V_q \end{pmatrix} = \begin{pmatrix} R_a & X_q \\ -X_d & R_a \end{pmatrix} \begin{pmatrix} I_d \\ I_q \end{pmatrix} \qquad (12)$$

where $X_d = \omega L_d$ is the direct axis reactance.

$X_q = \omega L_q$ is the quadrature axis reactance.

The voltage balance equation (12) suggests a phasor diagram for the parametric motor as shown in fig. 2, from which the following relations can be written:

$$\left.\begin{aligned} V_d &= V\sin\delta \\ V_q &= V\cos\delta \end{aligned}\right\} \qquad (13)$$

where δ is the load angle in electrical degrees.

Solving equation (12) for I_d and I_q one gets:

$$\left.\begin{aligned} I_d &= \frac{1}{\Delta}\left(R_a V_d - X_q V_q\right) \\ I_q &= \frac{1}{\Delta}\left(X_d V_d + R_a V_q\right) \end{aligned}\right\} \qquad 14)$$

where $\Delta = R_a^2 + X_d X_q$

Consequently the motor phase current is given by:

$$I = \sqrt{I_d^2 + I_q^2} \qquad (15)$$

The power factor can also be calculated from the relation:

$$\cos\phi = \sin(\psi - \delta) \qquad (16)$$

III-2 Torque Expression

The speed voltage coefficient matrix $\mathbf{G}$ can be written from either (11) or (12). The elements of $\mathbf{G}$ are the coefficients of the electrical angular speed ω_r. Considering equation (1), $\mathbf{G}$ matrix is given by:

$$\mathbf{G} = \begin{pmatrix} 0 & L_q/2 \\ -L_q/2 & 0 \end{pmatrix} \qquad (17)$$

The air-gap torque exerted by the motor is given by :

$$T_g = \frac{3}{2} P\,\mathbf{I}'^T\mathbf{G}'\mathbf{I}'$$

$$= -\frac{3}{4} P\left(L_d - L_q\right) I_d I_q \qquad (18)$$

The torque can be expressed in terms of δ by using (13), (14) and (18) in the following form:

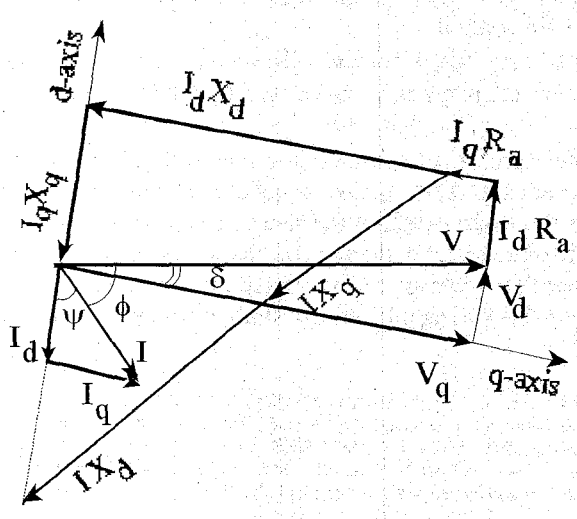

Fig. 2 Phasor diagram of three phase parametric motor

$T_g(\delta) =$

$$\frac{P}{8}\left(\frac{V}{\cos\phi_R}\right)^2 \frac{L_d - L_q}{Z_d Z_q}\left\{\sin\left(\phi_d + \phi_q - 2\delta\right) - \sin\phi_R\right\} \quad (19)$$

where: $Z_d = \sqrt{R_a^2 + X_d^2}$, $Z_q = \sqrt{R_a^2 + X_q^2}$,

$\phi_d = \tan^{-1}\left(X_d/R_a\right)$, $\phi_q = \tan^{-1}\left(X_q/R_a\right)$ and

$$\phi_R = \phi_d - \phi_q$$

From (19) the torque equals zero at δ_o such that:

$$\delta_o = \phi_d - \pi/2 \quad (20)$$

Also maximum output torque can be obtained at δ_m such that:

$$\delta_m = \frac{\left(\phi_d + \phi_q\right)}{2} - \frac{\pi}{4} \quad (21)$$

The maximum torque T_m is given by:

$$T_m = \frac{3}{8} P \frac{V}{\cos\phi_R} \frac{L_d - L_q}{Z_d Z_q}\left\{1 - \sin\phi_R\right\} \quad (22)$$

The equations obtained above are similar to that obtained for the reluctance motor. This ensures that a parametric machine can be treated as a hypothetical reluctance machine of half the number of poles provided that the machine parameters (especially direct and quadrature axes inductance) are properly defined. This is owed to that the period of phase inductance variation is 360 electrical degrees compared with 180 in the reluctance machines [5]. Therefore, it is important to note that for P-pole parametric machines, the relation between mechanical and electrical evaluation of angles (δ,ψ,...,etc.) differs from that for synchronous and reluctance machines. For the present machine:

Angle in elect. deg. = (P/4) angle in mech. deg. (23)

IV- Experimental Verification

In order to check the validity of the mathematical model described in the previous sections, an experimental study has been carried out.

IV-1 Experimental Setup

A three-phase slip-ring induction motor was used as a parametric motor by series connection of the stator and rotor windings with proper phase sequence. The machine data are given in the Appendix section

A dc machine was mechanically coupled to the induction motor to provide a mechanical load when operated in the generator mode. The dc machine was used also in the motor mode to facilitate the starting of the parametric motor in a similar way to that used in starting the synchronous motors. The speed was measured using an ac tachometer.

IV-2 Axes Inductances Measurement

Axes inductances L_d and L_q were determined using the method described in [4,5]. To simulate the saturation effects, L_d and L_q were measured at different values of axes currents I_d and I_q defined in the phasor diagram shown in fig. 2 by:

$$\left.\begin{aligned} I_d &= I\cos\psi \\ I_q &= I\sin\psi \end{aligned}\right\} \quad (24)$$

It was found that L_d is nearly constant in the operating range and equals 1.2 H while L_q is highly affected by I_q. Fig. 3 shows the experimental relation between L_q and I_q as well as a suitable curve fitting described by the following relations:

$$\left.\begin{aligned} L_q &= 0.034\left\{1 - e^{-2I_q}\right\} \text{ H} \quad \textit{for} \quad I_q < 3\text{A} \\ &= -0.004\, I_q + 0.046 \text{ H} \quad \textit{for} \quad I_q > 3\text{A} \end{aligned}\right\} \quad (25)$$

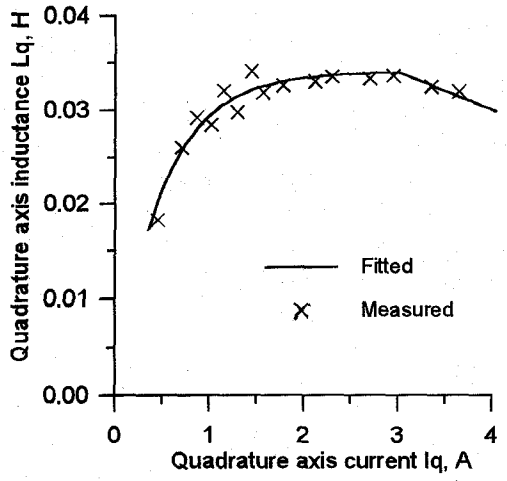

Fig. 3 Effect of magnetic saturation on the quadrature axis inductance.

V- Results and Discussion

A set of experimental tests have been carried out at an applied line voltage of 216 V (at no-load). The frequency was 40 Hertz such that the running speed was 2400 r/min. Since the motor is not self-started, so the roror was accelerated by the dc machine to a speed slightly higher than the operating speed. Then the dc machine was swithched off. In the same time the supply voltage was switched on. The results can be classified into the following groups of curves:

- ***Load angle characteristics***

Figure 4 shows the relation between load angle δ and both of output torque T_o and phase current I, while fig. 5 shows the relation between δ and input power P_{in}. It is noted that pull-out occurs when δ exceeds 14 elect. deg. Fig. 6 shows the relation between δ and both of power factor and efficiency. Power factor is nearly constant while efficiency increases up to δ= 8 elect. deg. and then tends to decrease.

- ***Output power characteristics***

Figure 7 shows the relation between output power P_{out} and input power P_{in}. Fig. 8 shows the relation between P_{out} and phase current I. Fig. 9 shows the relation between P_{out} and both of the input power factor and efficiency.

- ***Current waveforms***

Figure 10 shows the experimental steady-state current waveform at output torque of 1.6 Nm. Figure 11 shows the current waveform at the instant of pull-out, while fig. 12 shows the current waveform after pull-out.

From the characteristic curves given in figs. 4-9, the following notes can be extracted:

1) The correlation between the experimental and theoretical results shows satisfactory agreement. This proves the validity of the suggested model.

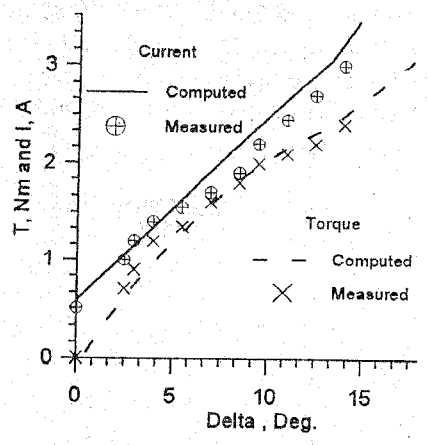

Fig. 4: Variation of both of the output torque T_o and phase current I against load angle δ

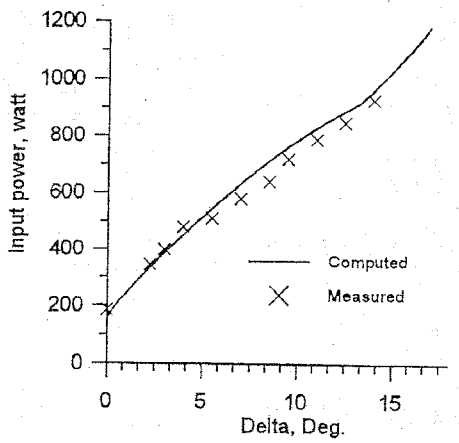

Fig. 5: Variation of the input power P_{in} against load angle δ

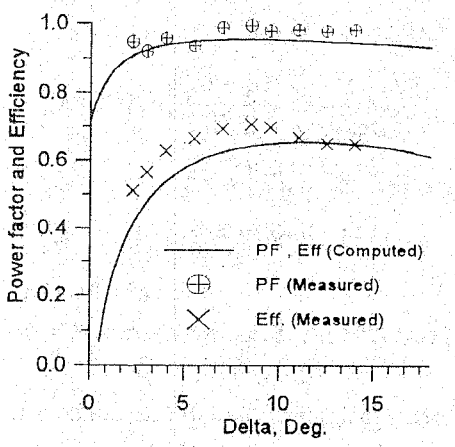

Fig. 6: Variation of both of the power factor and efficiency against load angle δ

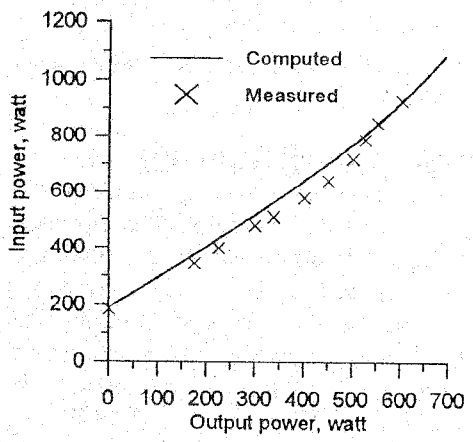

Fig. 7 : Variation of the input power P_{in} against output power P_{out}

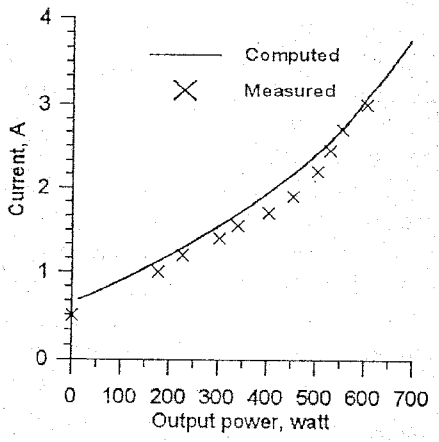

Fig. 8 : Variation of the phase current I against output power P_{out}

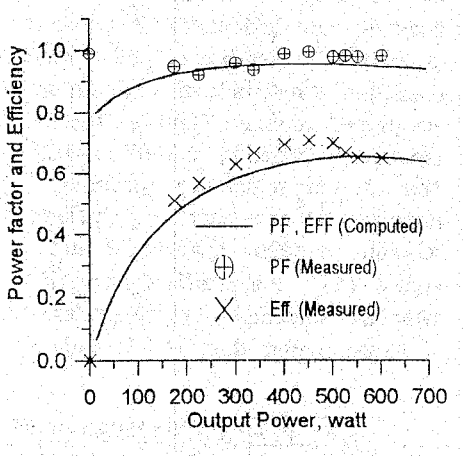

Fig. 9 : Variation of both of the power factor and efficiency against output power P_{out}

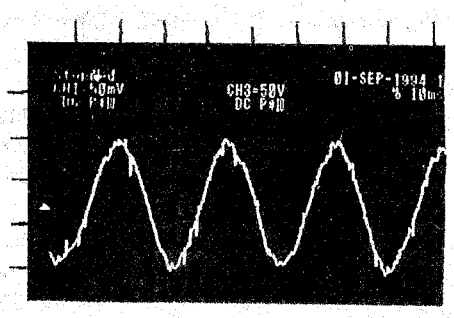

Fig. 10 : Steady-state current waveform at T_o=1.6 Nm. Scale : 50 mV/Div. 1mV=0.03 A

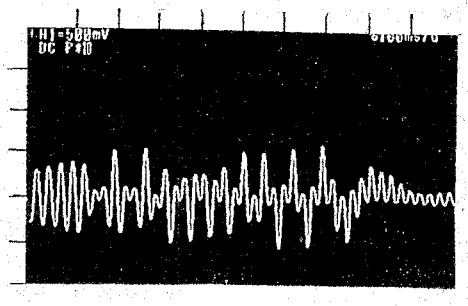

Fig. 11 : Current waveform at pull-out of synchronism. Scale : 500 mV/Div. 1mV=0.03 A

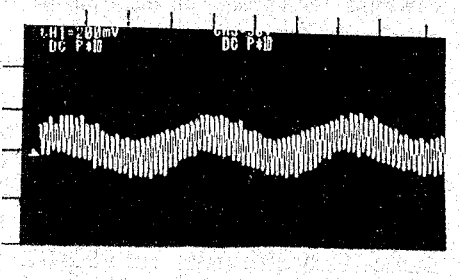

Fig. 12 : Current waveform after pull-out of synchronism. Scale : 200 mV/Div. 1mV=0.03 A

2) The pull-out occurs when the current exceeds about 3A. It was found that this limit is approximately the same for different values of the applied voltage. This can be attributed to the saturation in the quadrature axis inductance. It was found that direct axis current I_d does exceed 0.4 A (approx.) due to the high value of X_d. This means that L_d does not saturate and that most of the winding current is in the q-axis. Figure 13 shows the theoretical relation between δ and I when considering saturation in L_q as described in section V-2 compared with the relation if L_q were not saturated, i. e. L_q approaches 0.034 H for $I_q > 3$ A. It is obvious that the reduction in L_q (due to saturation) results in an increase in the winding current causing a further reduction in L_q, and so on. The process continues until the unstable region in the torque-δ characteristics is reached resulting in pull-out of synchronism. The experimental current waveform at pull-out given in fig. 11 shows that the pull-out occurs after a rapid increase in current. Figure 12 shows that the current waveform after pull-out exhibits unstable behavior. It was found that, in this mode, the motor speed reduces to slightly less than the synchronous speed even if the load is reduced. The torque produced in this case may be due to the eddy currents and/or the induced emf in the rotor phases resulting in an operation similar to that of the induction motor with low stable range.
3) The power factor is in general high. This is owed to that the ratio L_d/L_q is high (over 40). This ratio corresponds to the saliency ratio in the reluctance machine. The L_d/L_q ratio in wound-rotor parametric machines increases with the increase in the rotor to stator turns ratio with an optimum value of unity [6].
4) The efficiency is acceptable although the employed motor was not designed for such a mode of operation.

The output power is low compared with the rated value. This is due to the use of low value of the applied voltage which can be increased to about 700 V because of the series connection of the stator and the rotor windings. Increasing the applied voltage will allow wider range of operation due to the reduction in the winding current for the same output power. This enables obtaining more amount of power (torque) in the unsaturated range for L_q ($I_q < 3$ A.). Figure 14 shows the theoretical T-δ curves for different values of the applied line voltage. It is noted that the torque at pull-out increases with the increase in the applied voltage.

VI- CONCLUSIONS

The steady-state performance of a wound rotor parametric motor has been studied theoretically and experimentally. The theoretical analysis is based on the transformation to d-q model taking the saturation effect into account. The results revealed that a parametric motor is in effect of synchronous type. It operates at a constant speed of double the synchronous speed of the stator and rotor mmfs. This means that the speed is determined by the number of poles and the supply frequency and it is independent of the load conditions in the stable range of operation.

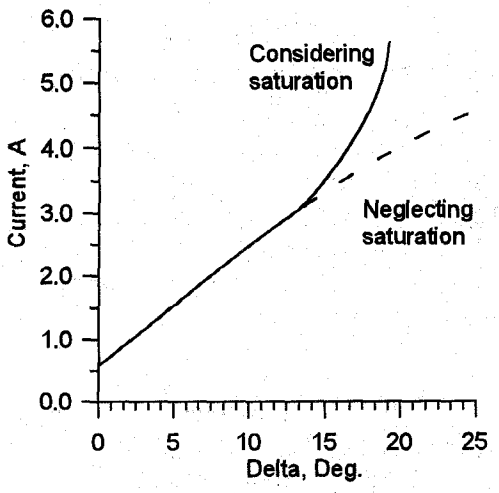

Fig. 13 Effect of saturation in L_q on the I-δ relation.

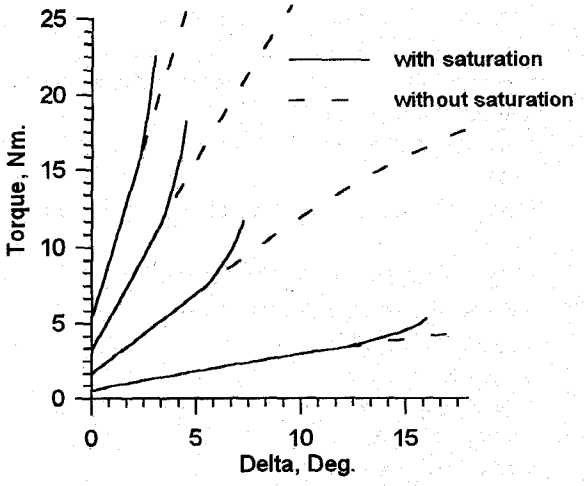

Fig. 14 Theoretical relation between T_g and δ for different values of the applied voltage.

The performance of the parametric motor is similar to that of the reluctance motor. The ratio L_d/L_q can be varied in the parametric motor by varying the stator to rotor turns ratio. This enables obtaining higher values for L_d/L_q compared with that obtained in the reluctance motor. In the present analysis L_d/L_q exceeds 40 for turns ratio of 0.86. Further increase can be achieved if the turns ratio approaches unity.

It was found that the pull-out of synchronism occurs when the quadrature axis inductance begins to saturate. Therefore the stable region can be controlled by controlling the saturation level in the q-axis. This can be done by controlling the applied voltage.

Comparison between experimental and theoretical results shows satisfactory agreement. It proves the validity of the mathematical modeling used.

The results can be considered as useful guides for operating and designing three-phase wound-rotor parametric motors.

The main disadvantage of the parametric motor is the absence of starting torque. Further study concerning this problem is being performed. The results will be presented in the near future.

APPENDIX

The data of the employed slip-ring induction motor are as follows:

Power : 2.2 KW, Frequency : 50 Hz, Speed : 1390 r/min
Stator 220/380 V , Δ/Y , 6.3/3.6 A
R_s=2.1 Ω/phase , X_s=5.28 Ω/phase
Rotor 328 V , Y-connected , 4.2 A
R_r=1.96 Ω/phase , X_r=3.92 Ω/phase
Rotor to stator turns ratio = 0.86

LIST OF SYMBOLS

v_d , v_q	direct and quadrature axes voltages, V.
i_d , i_q	direct and quadrature axes currents, A.
V	terminal phase rms voltage, V.
V_L	terminal line rms voltage, V.
I	phase rms current, A.
R_s ,R_r	stator and rotor phase resistances, Ω.
L_s ,L_r	stator and rotor phase self inductances, H.
M	max. mutual inductance between one stator phase and one rotor phase, H.
θ	electrical angle between stator phase 'a' and rotor phase 'a'.
ω	electrical angular frequency of the supply voltage, rad/s.
ω_r	electrical angular rotor speed, rad/s.
δ	electrical load angle, rad/s.
T_g	air-gap torque, Nm.
T_o	output torque, Nm.
P_{out}	output power, W.
P_{in}	input power, W.
P	number of motor poles.
p	differential operator d/dt.

REFERENCES

[1] A. S. Mostafa, Ph.D. Thesis, Cairo University, May 1946

[2] E. M. Rashad, "Parametric Generator ", M.Sc. Thesis, Alexandria University, Sept. 1987

[3] E. M. Rashad, "Application of Floquet's theory to the analysis of parametric generator" , Ph.D. Thesis , Alexandria University, Oct. 1992.

[4] A. S. Mostafa, A. L. Mohamadein and E. M. Rashad, "Analysis of series-connected wound-rotor self-excited induction generator", IEE Proc. B , Vol. 140, No.5, Sept. 1993.

[5] A. S. Mostafa, A. L. Mohamadein and E. M. Rashad, "Application of Floquet's theory to the analysis of series-connected wound-rotor self-excited synchronous generator", IEEE Trans. on EC, Vol. 8, No. 3, Sept. 1993.

[6] A. L. Mohamadein and E. A. Shehata, "Theory and performance of series-connected self-excited synchronous generator" , IEEE Trans. on EC, Vol. 10, No. 3, Sept. 1995

[7] Y. G. Desouky, "Voltage control of series-connected self-excited synchronous generator" M.Sc. Thesis , Alexandria University, Oct. 1993.

[8] M. M. El-Shanawany, "Capacitor controlled self-excited series-connected synchronous generator", Eng. Research Bulletin , Faculty of Eng. Menoufia University, Vol. 17, Part I, 1994.

[9] N. N. Hancock, "Matrix analysis of electric machinery" Pergamon, 2ed .Edition, .1974

BIOGRAPHY

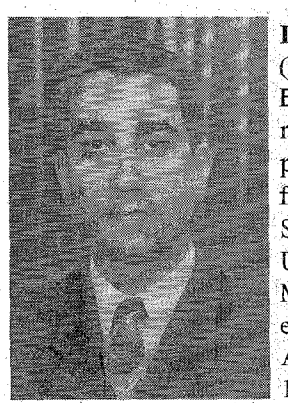

Dr. Essam El-Din M. Rashad (M94) was born in Shebin El-kom, Egypt on Sept. 1960. In 1983, he received B.Sc. degree in electrical power and machines engineering from Faculty of Engineering, Shebin El-Kom, Menoufia University, Egypt. He received M.Sc. and Ph.D. degrees both in electrical engineering from Alexandria University, Egypt in 1987 and 1992 respectively. From 1985-90 he was an offshore electrical engineer in Belayim Petroleum Company, Abo-Rudies fields, Sinai, Egypt. In 1990 he joined Ministry of Higher Education, Egypt as an engineering education lecturer. In 1992 he was appointed as an assistant lecturer in the electrical engineering department, Faculty of Engineering, Tanta University , Egypt. In 1993 he was promoted a lecturer in the same department

Dr. Mostafa E. Abdel-Karim was born in Kallin, Kafr El-Sheikh, Egypt on Dec. 1958. He received B.Sc., M.Sc. and Ph.D. degrees all in electrical engineering from faculty of engineering , Shebin El-Kom , Menoufia University, Egypt in 1981, 1985 and 1991 respectively. From 1987 to 1990 he was a channel system member in I.N.P.L. Nancy, France. In 1981 he was appointed as a demonstrator in the electrical engineering department, Faculty of Engineering, Shebin El-Kom, Egypt. From 1985 to 1991 he was an assistant lecturer in the same department where he is now a lecturer. His research interest includes power electronics, electrical machines and automatic control systems.

Mr. Yasser G. Desouky received B.Sc. and M.Sc. both in electrical engineering from Faculty of Engineering , Alexandria University, Egypt in 1991 and 1993 respectively. In 1991 he joined the Arab Academy for Science and Technology, Miami, Alexandria, Egypt as a demonstrator. Since 1994 he is working toward Ph.D. degree from Heriot-Watt University, Edinburgh, United Kingdom.